Biosensors and Bioelectronics 180 (2021) 113115

Contents lists available at ScienceDirect

Biosensors and Bioelectronics

journal homepage: http://www.elsevier.com/locate/bios

Utilizing pulse dynamics for non-invasive Raman spectroscopy of blood analytes

Maciej S. Wróbel [a,*], Jeong Hee Kim [b], Piyush Raj [b], Ishan Barman [b,c,d], Janusz Smulko [a]

[a] Department of Metrology and Optoelectronics, Faculty of Electronics, Telecommunications, and Informatics, Gdańsk University of Technology, G. Narutowicza 11/12, 80-233, Gdańsk, Poland
[b] Department of Mechanical Engineering, Johns Hopkins University, Baltimore, MD, 21218, USA
[c] Department of Oncology, The Johns Hopkins University School of Medicine, Baltimore, MD, 21287, USA
[d] The Russell H. Morgan Department of Radiology and Radiological Science, The Johns Hopkins University School of Medicine, Baltimore, MD, 21287, USA

ARTICLE INFO

Keywords:
Blood constituent monitoring
Raman spectroscopy
Turbid media
Modulation techniques
Optical diagnostics
Glucose

ABSTRACT

Non-invasive measurement methods offer great benefits in the field of medical diagnostics with molecular-specific techniques such as Raman spectroscopy which is increasingly being used for quantitative measurements of tissue biochemistry *in vivo*. However, some important challenges still remain for label-free optical spectroscopy to be incorporated into the clinical laboratory for routine testing. In particular, non-analyte-specific variations in tissue properties introduce significant variability of the spectra, thereby preventing reliable calibration. For measurements of blood analytes such as glucose, we propose to decrease the interference from individual tissue characteristics by exploiting the known dynamics of the blood-tissue matrix. We reason that by leveraging the natural blood pulse rhythm, the signals from the blood analytes can be enhanced while those from the static components can be effectively suppressed. Here, time-resolved measurements with subsequent pulse frequency estimation and phase-sensitive detection are proposed to recover the Raman spectra correlated with the dynamic changes at blood-pulse frequency. Pilot *in vivo* study results are presented to establish the benefits as well as outline the challenges of the proposed method in terms of instrumentation and signal processing.

1. Introduction

Non-invasive methods for medical diagnostics are greatly sought after as they offer a painless and convenient route with reduced risk of infections and the possibility for continuous monitoring, particularly if developed in a miniaturized and/or wearable format (Zhou et al., 2020). In this context, one of the key themes in biophotonics research has been the development of a reliable non-invasive blood glucose sensor. Numerous innovative designs to replace conventional fingerstick testing for glucose measurements have been proposed and tested with varying degrees of success (Aggidis et al., 2015). Label-free optical methods have attracted considerable attention due to the potential of nonperturbative measurements and simultaneous analysis of other blood constituents with minimal change in the employed method (Tuchin, 2008; Wang et al., 2018). Combining the penetration depth of near-infrared (NIR) light and molecular fingerprinting capability, vibrational Raman spectroscopy has offered promising results (Pandey et al., 2017). Many laboratories, including our own, have focused on harnessing and advancing Raman spectroscopy through studies in samples of progressively higher complexity (Wróbel 2016; Spegazzini et al., 2014; Scholtes-Timmerman et al., 2014). However, despite many successful proof-of-concept studies (Pandey et al., 2017), key challenges persist with various adverse impacts on the calibration of such systems (Lipson et al., 2009). While a single-patient calibration has been successfully shown (Singh et al., 2018; Barman et al., 2012), there remain significant calibration challenges due to individual (non-analyte specific) variability of physical (optical properties, dimensions of skin layers, vessels and capillaries, subcutaneous fat, etc.) and chemical (specific chemical composition of skin and blood) properties of the tissues.

Such individual variability introduces spectral perturbations, which may not be easily detected and separated by existing noise removal methods (Kang et al., 2020; Smulko et al., 2014). The method for isolating and reducing the influence of the optical properties (reduced scattering coefficient μ_s', and absorption coefficient μ_a) of skin on the spectra, termed turbidity-correction, has been previously proposed (Barman et al., 2011). It was based on the simultaneous detection of

* Corresponding author.
E-mail address: maciej.wrobel@pg.edu.pl (M.S. Wróbel).

https://doi.org/10.1016/j.bios.2021.113115
Received 24 September 2020; Received in revised form 22 February 2021; Accepted 23 February 2021
Available online 26 February 2021

diffuse light scattering and the Raman scattering signals and using the former for the correction of the spectral shape of the latter. The method is effective in a limited range of μ_a and μ_s'. Other investigators have proposed a tissue modulation approach (Chaiken et al., 2001), where a spatiotemporally localized mechanical stimulus is employed to manipulate the mobile components of tissue relative to the static components, and difference spectroscopy is subsequently used to isolate the spectra of the two. This modulation provides spectra that are primarily representative of the blood constituents, which are used to correct the bulk tissue spectral measurements and improve the Raman calibration for glucose detection (Chaiken et al., 2005). Another NIR measurements-based glucose detection scheme utilizes pulse-induced blood volume changes, which is conceptually the closest to our idea, to establish the attenuation baseline, which is used for spectral correction (Yamakoshi and Yamakoshi, 2006).

By leveraging established concepts in signal processing and Raman spectroscopy, we propose a novel method for identifying the component of the Raman spectrum generated mainly by the blood cells and plasma constituents. A combination of concepts from these disparate fields of knowledge allows us to develop a method with prospects for greater specificity for the detection of blood constituents based on acquired Raman spectra.

Our proposed solution to this problem is based on the utilization of the naturally occurring blood pulse and the difference in optical parameters between red blood cells and other tissue components. The heart rhythm provides pulsation to the blood cells flowing through the vessels, which scatter the excitation of laser light. This gives rise to a modulated signal, where the modulation depends on the blood flow parameters and is largely unaffected by the parameters of the surrounding tissue matrix. We reason that the blood signal will contribute to the dynamic component of the spectrum, while the tissue matrix components (skin, muscle, vessel walls, fat, etc.) will provide the static component of the Raman spectrum. Our analysis is focused on the detection of the pulse frequency and the filtering of the periodical signal with a digital phase-detection algorithm, resulting in the estimation of the pulse-correlated Raman signal. This method should, in principle, be more independent from patient-specific variations because optical parameters and chemical composition of blood are much more consistent over the human population of different races and ages than that of the surrounding solid tissue. Our approach has numerous advantages over the method utilizing mechanical tissue modulation. It is worth emphasizing that the measurements utilizing natural blood pulse can be recorded for a longer time to assure better averaging and noise reduction. Besides, mechanical modulation is dependent on the tissue stiffness and viscoelasticity and hence likely to be more influenced by biological variability; furthermore, such modulation may disturb the natural blood flow in unpredictable ways.

Here, we present experimental results of *in vivo* Raman spectroscopic measurements from human subjects, and methods to estimate the blood spectral signatures from the pulse-modulated signal over time. We have used a Raman spectrometer with an 830 nm excitation wavelength and a fiber-optical probe designed for contact measurements. We have measured the signal with a high sampling frequency (10 Hz sampling rate) to satisfy the Nyquist criterion for probing the blood pulse signal (that should be contained in about 0.75–1.5 Hz bandwidth) continuously for 10 min. We have subsequently applied signal-processing methods to the recorded spectra to determine the regions in the Raman spectrum that are strongly correlated to the changes in blood volume over time. We have identified the dominant blood pulse frequency and recovered the Raman signal correlated with the pulse dynamics. These results have broader implications for clinical translation of Raman spectroscopy-based blood analyte monitoring and for other biological applications where sample-to-sample variability in tissue composition could undermine the predictive ability of developed chemometric models. Additionally, our approach may offer further insights into the dynamics of recorded pulse changes, their potential correlation to specific analyte concentrations and disease states, and the ability of optical spectroscopy to diagnose such complications.

2. Materials and methods

2.1. Detection scheme

Here we present the proposed detection scheme (Fig. 1), based on the synchronous detection (or phase-sensitive) algorithm, similar to the generally known one from the lock-in amplifier principle. However, a key difference is that the reference signal $R(t)$ is not generated but is detected from the blood pulsation. The Raman spectrum $S(n, t)$ is registered continuously at selected times t and for Raman shifts n with high speed and over substantial observation time, to record multiple samples of a time-varying signal, with multiple periods of the blood pulse. First, the dominant blood pulse frequency f is detected. We determine this frequency by estimating the power spectral density (PSD) of the Raman spectra time series, which was averaged over Raman shifts, to reduce its random error. The frequency responding to a local maximum in about 0.75–1.5 Hz bandwidth determines blood pulse frequency.

Then, this frequency f is used to create in-phase (P) and quadrature (Q) components of the reference harmonic signal $R(t)$, which are used in the algorithm (Fig. 1). This procedure is performed separately for each of the discrete Raman shifts n (corresponding to each pixel column of the CCD camera), recorded by the Raman spectrometer. Fig. 1c presents the blocks of data processing in an algorithm of a lock-in amplifier to estimate the intensity of the harmonic carrier signal of frequency f in the analyzed Raman spectra. Data processing requires averaging, represented by an operator $E[\cdot]$, of the products of Raman spectrum and P or Q components: $E[S(n, t)\cdot P]$ and $E[S(n, t)\cdot Q]$. The averaged product $E[S(n, t)\cdot S(n, t)]$ is a variance of the recorded Raman spectra at selected Raman shift n, and is used for data scaling in the lock-in algorithm (Kotarski and Smulko, 2009). The output of the applied lock-in algorithm is an amplitude of the component (carrier signal) extracted from the recorded Raman spectra of the frequency f and related to blood pulse. We can estimate a phase shift between the reference signal $R(t)$ and the carrier signal component in the Raman spectrum, but this value has not been used for our analysis.

The blood pulse can be represented by a sum of at least a few harmonic components. Moreover, the frequency f at the local maximum in the PSD of the recorded Raman spectra is identified with a limited accuracy due to the frequency resolution of the estimated PSD and spectrum leakage effect. We propose to reduce these effects by repeating the algorithm of the lock-in amplifier multiple times with slightly changed center frequency within the width of this band of increased intensity. This procedure takes into account the experimentally recorded pulse rate within the identified frequency range. The results recover many instances of the pulse-correlated Raman spectrum, which are then averaged to reduce the noise caused by the overall low signal levels. The optimal number of instances to be averaged to reduce noise requires in-depth analysis and depends on the measurement setup (e.g., the integration time of recorded Raman spectra, sampling frequency, number of the recorded spectra) and experimental data (e.g., the stability of blood pulse and mechanical stability of the Raman probe irradiating skin tissue). Because of various factors, we chose to repeat the implementation of the lock-in amplifier algorithm to maximize signal-to-noise ratio – SNR. Thus, we arrive at a final Raman spectrum, which contains more information related to the signal of the periodically changing blood levels, and less related to the static background of the tissues. The last operation on the resulting Raman spectra is Savitzky-Golay filtering using a polynomial of the 5th order with 20 points window for averaging to reduce noise.

The noise component in the recorded Raman spectra is very intense, and therefore, we proposed to consider their masking to reduce its influence before applying the PSD algorithm. Masking should expose more

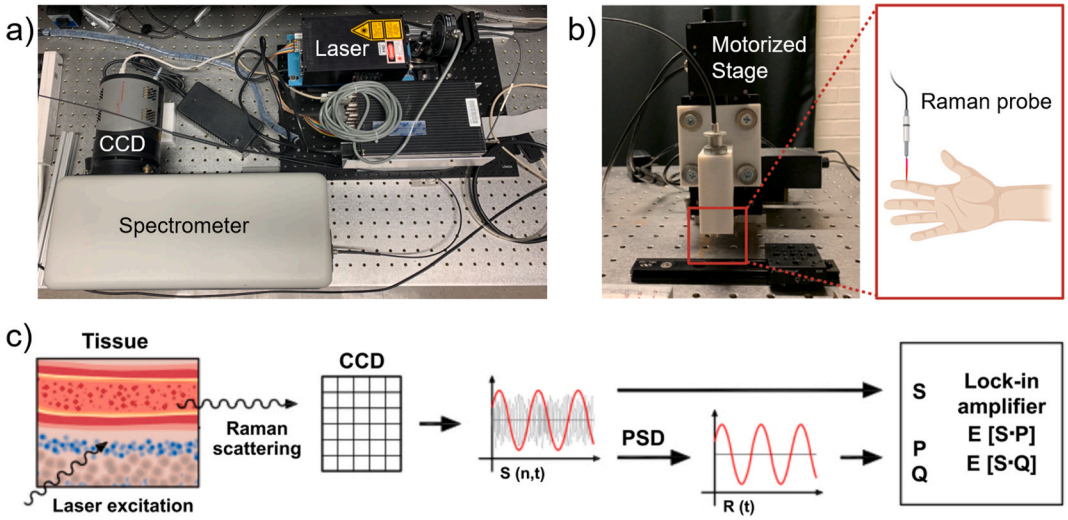

Fig. 1. The scheme of the detection method and measurement setup. (a) the Raman spectrometer setup. (b) The fiber optic probe and fingertip positioning. (c) The scheme of the detection method. The laser irradiated tissue emits Raman scattered light which is recorded by the CCD detector as the Raman spectra *S(n,t)*. Raman spectra *S*(*n*, *t*) are recorded in the time *t* domain at each Raman shift *n*. The heart acts as a reference generator of harmonic signal (red line) representing blood pulse. The frequency *f* of blood pulse is derived from power spectral density (PSD) of *S*(*n*, *t*) and is used to generate *R*(*t*) for synchronous detection algorithm. The reference signal *R*(*t*) is decomposed into two parts: in-phase *P* (*P* = *R*(*t*)) and its quadrature version *Q* shifted by 90°; both components are utilized in further processing to make the algorithm independent from the phase shift introduced by the tissue. The end result is the part of a Raman spectrum *S*(*n*, *t*), which is correlated with the original blood pulse frequency *f*. Operator *E*[·] means averaging. Lines and arrows represent the direction of data processing. (For interpretation of the references to colour in this figure legend, the reader is referred to the Web version of this article.)

efficiently the component related to blood pulse and attenuate noise components in the parts of Raman spectra related to tissue or representing noise generated mainly by the applied CCD sensor. We propose to consider [0 to 1] mask of Raman spectra at selected Raman shifts. The promising candidates are the most prominent bands for hemoglobin or the Raman band above 800 cm^{-1} (based on the a priori information of observation of a pulse signal in Raman measurements (Chaiken et al., 2009)).

Thus, we have three approaches to Raman spectra masking:

1. *Original spectrum integration.* PSD estimates were calculated for each pixel of the recorded Raman spectrum in the range 400–1800 cm^{-1} of Raman shifts and integrated to obtain final PSD.
2. *Spectrum masking.* We have constructed a [0 to 1] intensity mask – Fig. 3a, with the spectral characteristics resembling the most prominent hemoglobin bands. The signal (Raman spectrum) was multiplied by the mask, and Welch's method was applied to obtain the PSD like in the previous case. The underlying rationale is that the volume of whole blood in a capillary should change significantly between systole and diastole phases of the heart rhythm.
3. *Inelastic spectrum integration.* Based on the a priori information of observation of a pulse signal in Raman measurements (Chaiken et al., 2009), we have applied the integration of the inelastic light scattering at the Raman band above 800 cm^{-1} prior to PSD estimation.

2.2. Measurement setup

The measurements were performed on a portable Raman spectrometer setup (Fig. 1), consisting of a spectrograph (Holospec f/1.8i), a TE-cooled CCD camera (PIXIS 400BR, Princeton Instruments), 830 nm laser, and fiber optic contact probe (EmVision, LLC.). The probe consists of one low-OH 300 μm, 0.22 NA, with a band-pass filter for excitation and seven such fibers for collection of the signal with a ring-shaped low-pass filter. The spot size is 500 μm in diameter at the contact point of the probe.

2.3. Measurement procedure

In vivo measurements on the fingertips of five healthy human volunteers were conducted to assess the performance of the measurement

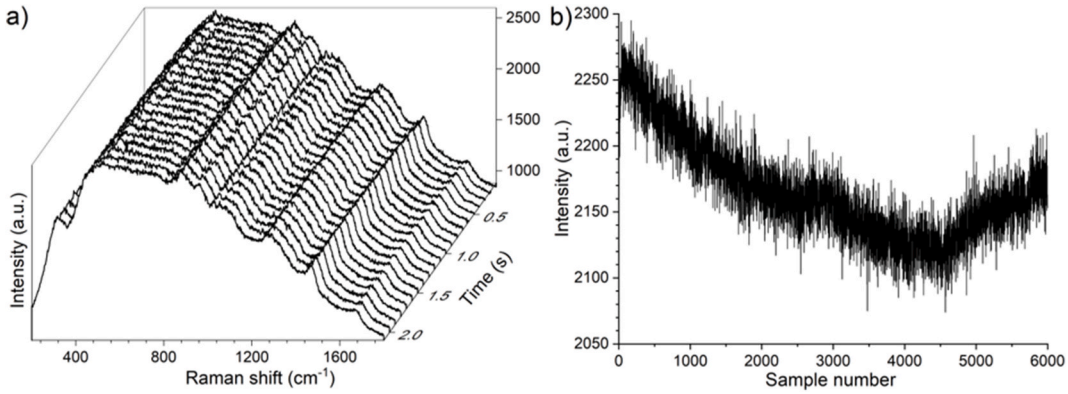

Fig. 2. Experimental *in vivo* Raman spectrum, (a) a time-resolved set of spectra; (b) example of a pixel corresponding to about 1000 cm^{-1} Raman shift of time-resolved *in vivo* signal.

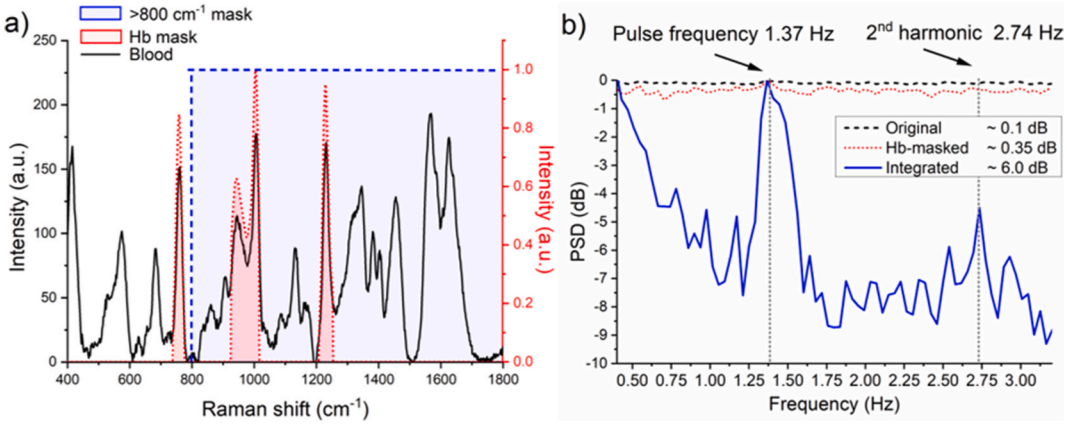

Fig. 3. (a) Spectrum of the selected Hb-mask overlaid over the representative Hb spectrum; (b) Resulting PSD (dB) estimation using three proposed methods: no integration (original), integration of inelastic scattered light, and after masking of Hb-specific features with the estimated values (dB) of signal-to-noise ratio (SNR) for each method. The SNR value is equal to the difference between the maximum of the PSD at 1.37 Hz and the averaged neighboring background level. The reference Hb spectrum was measured from Hb extracted from the lysed red blood cells. The Hb-mask was limited to the four most prominent Hb bands. (For interpretation of the references to colour in this figure legend, the reader is referred to the Web version of this article.)

setup and the signal processing performance for evaluation of the proposed method. These measurements were undertaken in pursuance of feasibility demonstration of the pulse-based non-invasive detection of blood analyte signals.

The *in vivo* experiment was performed in the following way. First, the hand of the patient was placed on a support to provide comfort and reduce possible muscle twitch and tremor, causing vibrations. The probe was placed on the fingertip, with a gentle yet steady contact, without any tissue compression. This provided a vibration-free measurement at the exact same spot over the fingertip for a prolonged amount of time. The laser power was set to about 50 mW at the end of the probe, which translates to the density of 50 W/cm^2 on the skin, approximately six times lower than in previously reported experiments (Dingari et al., 2011). The volunteers did not experience any pain nor reported any heating. The study was conducted in accordance with the protocol approved by the Independent Bioethics Committee for Scientific Research at the Medical University of Gdańsk no. NKBBN/469/2012.

3. Results

3.1. Raman spectra

The Raman spectra collected at 10 Hz rate (0.1 s integration time) are presented in Fig. 2a. Fig. 2b presents the temporal behavior of the signal for one recorded CCD pixel column as a function of time.

3.2. Data processing

Data processing was pursued to condition the signal to determine the presence of a periodic signal in the time-resolved measurements by using Welch's method to estimate PSD. Later, our algorithm, utilizing phase-sensitive detection (Fig. 1), was applied to extract the part of the Raman spectrum correlated with the estimated blood pulse signal.

3.2.1. Estimation of power spectral density

Three approaches, as mentioned above (in section 2.1), namely: no masking at all, excluding all bands except the selected hemoglobin bands, attenuating by masking by 0 the bands below 800 cm^{-1} were compared for signal conditioning to retrieve the pulse frequency by applying Welch's method. In all cases, Welch's method used a fast Fourier transform (FFT) of 256 samples length with a segment length of 256 and overlapping of 64 samples, while the total number of samples was 6000 (10 min of the measurements at sampling frequency $f_s = 10$ Hz). The parameters determined PSD for the frequencies with an interval between successive values equal $\Delta f = f_s/256 \approx 0.039$ Hz.

The recorded *in vivo* spectra exhibited a slowly time-varying signal due to movement artifacts and drops in total signal strength for the initial samples, most likely due to photobleaching. This results in a strong signal at DC and low-frequency components. The resulting PSDs are presented in Fig. 3b. The use of the original spectrum shows a very minimal signal concentrated around a frequency corresponding to the pulse rate (1.37 Hz), of about ~0.1 dB SNR (signal-to-noise ratio). The masking of hemoglobin spectra provides an improvement in the basic pulse frequency estimation, with 0.35 dB of SNR at the same peak frequency of about 1.37 Hz.

The integration of inelastically scattered light at above 800 cm^{-1} provides much better estimates, at about 6 dB of SNR at the same frequency (Fig. 3b). Also, a second harmonic becomes evident at 2.74 Hz. This result is important and has substantial implications for further spectral analysis. It echoes a similar finding in [13], but our approach does not require the use of any mechanical pressure, which could induce additional non-analyte-specific variations in the Raman signal. To the best of our knowledge, this represents the first Raman spectroscopy-based attempt to detect the blood pulse and subsequently utilize the same to decode Raman spectra acquired from the blood-tissue matrix.

The full-width at half-maximum (FWHM) at the base frequency is about 0.4 Hz, which may indicate that pulse frequency shows small changes over the time of measurement and that there are variations in blood pulse wave transit time over the irradiated fingertip area. Accuracy of the PSD estimation, and the estimated FWHM at 1.37 Hz, is also affected by spectral leakage in fast Fourier transform and the short length of the recorded signal overall. An intense signal at low frequencies is due to a static background signal and slow movements of the finger (much slower than the pulse rate). Some of these adverse effects can be reduced by better stabilization of finger position. The physiological and unavoidable changes of a pulse rate during the measurement can be considered in the more advanced algorithm when the pulse is monitored by applying an independent method such as photoplethysmography.

3.2.2. Retrieval of pulse-related Raman spectrum with phase-sensitive detection

The knowledge of the basic frequency (~1.37 Hz, or about 82 beats per minute – Fig. 3b), at which the blood-pulse-related changes are most evident, permits the use of the phase-sensitive (or lock-in) detection scheme (Kotarski and Smulko, 2009). In our case, the recorded temporal Raman signal is considered as a component induced by Raman scattering in the blood-tissue matrix, and having the identified pulse

frequency f, an additive noise component (random signal uncorrelated with the pulse wave, representing all the noise sources), with the slowly changing part representing tissue background. Using a digital phase-sensitive detection algorithm, the identified basic pulse frequency was used to create the reference harmonic signal $R(t)$, which is a component of the measured Raman spectrum $S(n, t)$ in time domain t at each Raman shift n, as shown in the schematic in Fig. 1. After low-pass filtering, the signal correlated with the base frequency is recovered, independently from the phase shift of the pulse signal introduced by the tissue. The time-domain signal is recovered for each pixel separately. Thus the output signal is a Raman spectrum correlated with the identified base frequency. To reduce the noise, the algorithm is run not only for the selected basic frequency of the reference harmonic signal $R(t)$ but also for multiple frequencies spanning the FWHM bandwidth of detected pulse frequency (±0.2 Hz) centered around the basic frequency 1.37 Hz (1.16–1.56 Hz). The number of 250 evenly distributed frequencies around 1.37 Hz was found to identify the spectrum component related to blood pulse in an optimal way for the considered data (via SNR value maximization), and the estimated PSD. We reasoned that the sum of harmonic signals could model the pulse, and the phase-sensitive detection was run separately for each of 250 frequencies. The results were averaged within the set of frequencies to reach a better SNR value. The number of frequency bins and bandwidth can be further optimized for better performance of the algorithm. Optimization depends on the time of signal recording, frequency resolution, and pulse stability during the experiment, though its detailed analysis was beyond the scope of the present study that focuses on the use of pulse signal to determine the component of Raman spectrum related to blood analytes. The quantitative comparison here is by employing SNR, since the final determinations of blood analyte concentration require the development of multivariate regression models. The latter step is identical for our approach as well as any existing pre-processing approaches that seek to improve the SNR for final quantification.

3.3. Algorithm results

The resulting final recovered spectrum is presented in Fig. 4a. It resembles the broadband fluorescence background with several Raman features visible from the skin input spectrum, such as at 300, 1245, 1440, and 1650 cm^{-1} (Pezzotti et al., 2015). Although overwhelmed by these broadband signals, a number of other bands can be clearly seen in the resulting spectrum, such as at 1050, 1195, 1416 cm^{-1}. Most of these bands can be attributed to whole blood and plasma (Atkins et al., 2017), while bands at 910, 1070, 1127, 1270, and 1377 cm^{-1} could be attributed to glucose (Kang et al., 2020). We present these results in Fig. 4b and c, comparing the measured Raman spectrum (averaged over 20 s) with the Raman spectrum resulting from the proposed algorithm and smoothed by Savitzky-Golay filtering. The data were normalized to the global maximum. Thus, we infer that the newly observed bands in the output spectrum can be considered as related to the changing blood volume over time at the rate of pulse frequency, which underscores the utility of the proposed method. A large number of peaks appeared in the 400–900 cm^{-1} region, however, due to larger noise contribution, they could not be precisely associated with specific blood components.

Additional measurements were conducted to assess the difference in method performance when comparing various skin melanin content (according to the Fitzpatrick scale for skin phototype (Sachdeva, 2009)), which expectedly impacts optical readouts. The results are compared in Fig. 4d–f for a human volunteer with skin phototype II (A) and volunteer with skin phototype IV (B). The results indicate lower PSD estimation

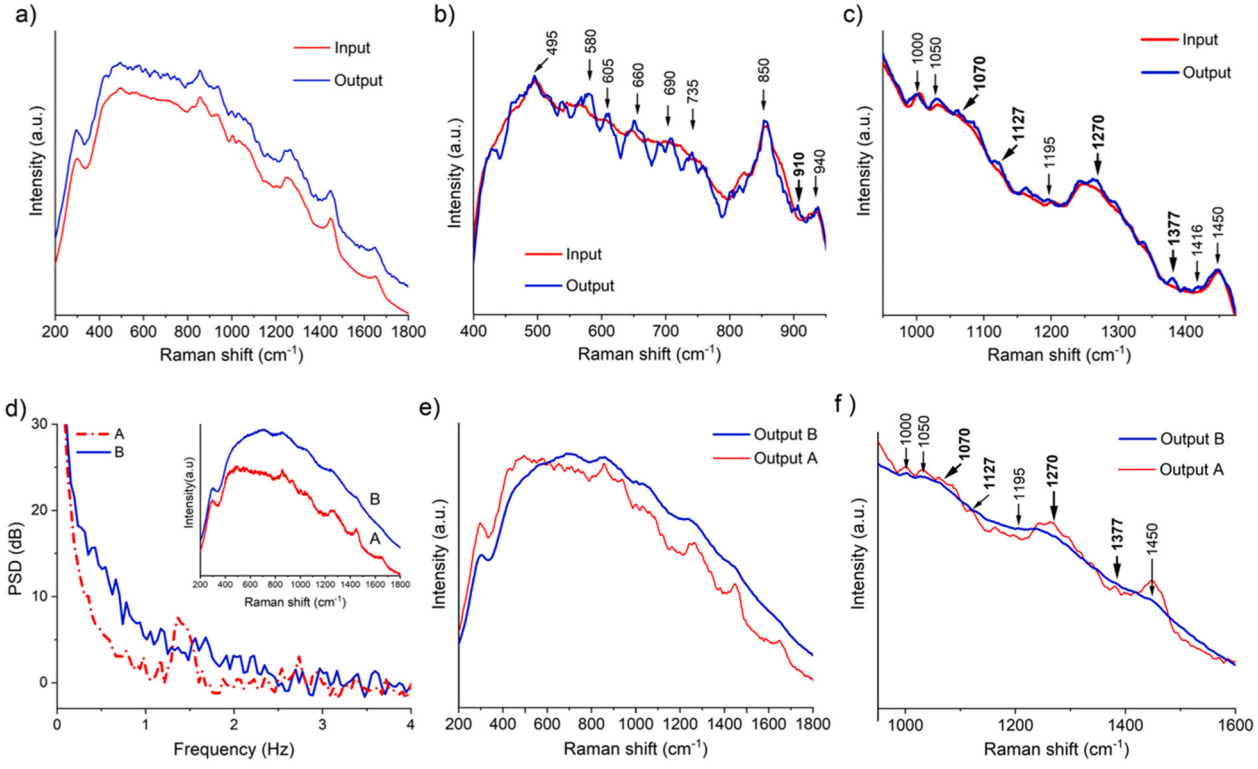

Fig. 4. Results of the phase-detection algorithm: (a) Raman spectrum of bulk tissue averaged over 20 s of the measurements – input (red) and the output spectrum correlated with pulse frequency (vertically offset for visualization purposes) (blue) obtained by the phase-sensitive detection; input (red) and output (blue) spectra in two regions of interest (b) 400–950 cm^{-1} and (c) 1000–1500 cm^{-1}, normalized to the selected local maximum value for better comparison. Important bands are marked with arrows, glucose-fingerprint regions are marked in bold. (d) Comparison of PSDs of Raman spectra signal for human volunteers A and B, with the inset showing recorded spectra. (e) Raman spectra after applying a phase-detection algorithm for phototype II (A) and phototype IV (B). (f) Region of interest showing similar peak positions for both human volunteer measurements. (For interpretation of the references to colour in this figure legend, the reader is referred to the Web version of this article.)

(Fig. 4d), with a maximum magnitude of 5.2 dB at 1.55 Hz for the second patient when compared with the base level, but low-frequency artifacts are more pronounced, resulting in an overall elevated PSD. Phase-sensitive detection algorithm yields a similar but more obscure spectrum (Fig. 4e) in comparison with the previous case, mostly due to the higher contribution of fluorescence in the original spectra (inset in Fig. 4d). Likewise, the background peaks are less clearly identifiable, while there are evident similarities with the blood spectral bands, appearing at the same Raman bands as for the patient with skin phototype II, zoomed-in Fig. 4f. We may conclude that skin type plays a crucial role in the intensity of the acquired Raman spectra. This effect, however, requires a more thorough analysis with an abundant number of volunteers, which will be the focus of our ongoing work.

4. Discussion

By applying the operation of a lock-in amplifier, we have identified the presence of and successfully isolated the pulse signal in Raman spectra recorded in human subjects. Our findings from this pilot study on a limited cohort of human subjects of various skin phototypes estimated the basic pulse frequency at approximately 1.37 Hz and 1.55 Hz for the studied patients, which ranges well within the typical blood pulse values. Normal blood pulse rates at rest for adults are typically between 0.98 and 1.65 Hz (59–99 beats per minute). Additional studies, presented in the supplementary information, confirmed that the basic pulse frequency, identified by Raman spectra processing, is very close to a simultaneous measurement obtained from a FitBit device (FitBit Inc., USA) positioned at the wrist. We have detected that there are specific bands of the spectrum which are more correlated with the blood pulse signal than others, such as the bands over 800 cm^{-1}, reflecting the most prominent blood bands observed in Hb (Fig. 3a). We note that the estimation of the pulse frequency may be slightly different from the actual value, due to factors notably the pulse wave transit time in capillaries in the irradiated skin volume and the change in patient heart rate during the measurement. This results in broadening of the pulse base frequency, with FWHM of about 0.4 Hz. The applied discrete Fourier transform (FFT algorithm) of the sampled Raman spectra is also responsible for the observed broadening due to the spectral leakage effect.

An application of the phase-sensitive detection allowed for the retrieval of the blood pulse correlated signal. The retrieved signal exhibits broadband changes rather than only singular spectral lines. One can reasonably infer that the resulting spectrum is due to a combination of multiple optical effects within the skin layers that correlate with the blood-tissue matrix dynamics. One such factor may be turbidity-induced variations, resulting in the loss of Raman signal strength, or change in fluorescence of blood and/or the bulk tissue. Additionally, red blood cells' aggregation-disaggregation in capillaries that changes the scattering coefficient may also play a role (Tuchin, 2008). Another factor, which may contribute to the retrieved spectrum, is the differential nature of oxy- and deoxy-hemoglobin spectra. Finally, the hemodynamic pressure that induces expansion of the vessels may interfere with the signal. It is important to note that the changes seen in the measured Raman spectra come from a probing volume that is approximately hemispherical in shape, with 0.5 mm diameter and *ca.* 1–2 mm depth (Agenant et al., 2014). This irradiated area consists of an ensemble of skin surface layer and subdermal region, interstitial fluid, capillaries filled with blood, etc., all of which contribute to the signal.

One significant advantage of this method over the tissue modulation approach (Chaiken et al., 2001) is the absence of external stimuli, which are associated with an inconsistent response of the modulated tissue, such as a difference in blood perfusion, tissue movements, and hysteresis of tissue deformation. Although our study considered originally the applicability of this method mostly for blood glucose concentration measurements, it opens up the possibility to measure other blood components as well, since it is the whole blood (plasma and blood cells) that undergoes dynamic volume changes with the pulse. The algorithmic procedure of exposing the part of Raman spectra related to red blood cells and plasma is valid for any component when modulated by blood pulse (the specific spectral lines and the background component induced by fluorescence). Hence, the proposed procedure can be further advanced by applying conventional methods such as noise filtering or background subtraction.

5. Conclusions

In this pilot experimental study, we have sought to elucidate the Raman spectra that are correlated with the blood pulse. By combining the well-established phase-sensitive detection method and utilization of a naturally occurring heart rhythm (as a reference frequency source for the detection algorithm), we were able to diminish the influence of the static tissue while enhancing the dynamic pulse-related Raman spectrum of blood. Such a method may pave the way for the non-invasive detection of numerous analytes of clinical importance through the skin. Our results show retrieval of the pulse frequency at 1.37 Hz, which is well within the clinical range. This represents the first determination of blood pulse, solely based on non-invasive Raman spectral measurements. Secondly, from the same measurements, we have retrieved the Raman signal showing multiple blood constituent-related spectral features. Similar results were achieved for other patients with distinct skin phototypes, underscoring the robustness of our developed method. The retrieved blood signal correlated with the pulse would be much clearer if the pulse-related signal was more intense, and pulse frequency was more stable. It is possible to improve this component of the Raman spectrum by mechanically stabilizing the part of the irradiated human body and optimizing the optical setup of collecting scattered light from the tissue. Spatially-offset Raman spectroscopy may be used to achieve this aim (Ma et al., 2011), along with improvements of other components such as a more quantum efficient camera and optical probe with higher throughput. It has been recently shown that using confocal collection (Lundsgaard-Nielsen et al., 2018) arrangement improves calibration for interstitial fluid glucose measurements due to the lack of interference from the surface tissue layers. This could also be utilized here to collect more intense signals to correlate with dynamic changes of tissue composition due to blood pulse. Direct observation of glucose bands was recently reported in a seminal study (Kang et al., 2020) utilizing transcutaneous Raman spectroscopy. We have found similar bands after applying our method, which may also indicate direct evidence for the presence of glucose bands in the pulse-correlated Raman signal of tissues.

The limitations of this pilot study surround the limited number of human volunteers on whom the measurements were performed, precluding a detailed statistical examination of the developed approach. We anticipate undertaking more comprehensive studies expanding on the current cohort of human subjects. Ultimately, we believe that the presented approach for Raman spectroscopy utilizing the blood pulse will form an important step in advancing such measurements for non-invasive medical diagnostics. Together with other recent advances in Raman spectroscopy for blood glucose determination (Lundsgaard--Nielsen et al., 2018; (Pleus et al., 2021), our approach should specifically accelerate the pursuit of a non-invasive and wearable blood glucose sensor.

Disclosures

The authors declare that there are no conflicts of interest related to this article. Results of this study partially constituted the PhD dissertation of corresponding author MW.

CRediT authorship contribution statement

Maciej S. Wróbel: Conceptualization, Methodology, Software,

Validation, Formal analysis, Investigation, Data curation, Visualization, Writing – original draft, Writing – review & editing, Funding acquisition. **Jeong Hee Kim:** Methodology, Validation. **Piyush Raj:** Methodology, Validation. **Ishan Barman:** Resources, Formal analysis, Writing – review & editing, Supervision, Funding acquisition. **Janusz Smulko:** Conceptualization, Validation, Formal analysis, Resources, Writing – review & editing, Supervision, Project administration, Funding acquisition.

Declaration of competing interest

The authors declare that they have no known competing financial interests or personal relationships that could have appeared to influence the work reported in this paper.

Acknowledgements

This study was supported by the National Science Center, Poland (NCN) under the grants 2016/20/T/ST7/00380 and 2017/25/N/ST7/01366; Foundation for Polish Science (FNP) START 95.2017; DS Programs of the Faculty of Electronics, Telecommunications and Informatics, Gdańsk University of Technology; CI TASK.

Appendix A. Supplementary data

Supplementary data to this article can be found online at https://doi.org/10.1016/j.bios.2021.113115.

References

Agenant, M., Grimbergen, M., Draga, R., Marple, E., Bosch, R., van Swol, C., 2014. Clinical superficial Raman probe aimed for epithelial tumor detection: phantom model results. Biomed. Optic Express 5 (4), 1203–1216.

Aggidis, A.G.A., Newman, J.D., Aggidis, G.A., 2015. Investigating pipeline and state of the art blood glucose biosensors to formulate next steps. Biosens. Bioelectron. 74, 243–262.

Atkins, C.G., Buckley, K., Blades, M.W., Turner, R.F.B., 2017. Raman spectroscopy of blood and blood components. Appl. Spectrosc. 71 (5), 767–793.

Barman, I., Dingari, N.C., Rajaram, N., Tunnell, J.W., Dasari, R.R., Feld, M.S., 2011. Rapid and accurate determination of tissue optical properties using least-squares support vector machines. Biomed. Optic Express 2 (3), 592–599.

Barman, I., Dingari, N.C., Singh, G.P., Soares, J.S., Dasari, R.R., Smulko, J.M., 2012. Investigation of noise-induced instabilities in quantitative biological spectroscopy and its implications for noninvasive glucose monitoring. Anal. Chem. 84 (19), 8149–8156.

Chaiken, J., Finney, W.F., Knudson, P.E., Peterson, K.P., Peterson, C.M., Yang, X., Weinstock, R.S., 2001. Noninvasive in-vivo tissue-modulated Raman spectroscopy of human blood: microcirculation and viscosity effects. Proc. SPIE 4254, 106–118.

Chaiken, J., Finney, W., Knudson, P.E., Weinstock, R.S., Khan, M., Bussjaeger, R.J., Hagrman, D., Hagrman, P., Zhao, Y., Peterson, C.M., Peterson, K., 2005. Effect of hemoglobin concentration variation on the accuracy and precision of glucose analysis using tissue modulated, noninvasive, in vivo Raman spectroscopy of human blood: a small clinical study. J. Biomed. Optic. 10 (3), 031111–031112.

Chaiken, J., Goodisman, J., Deng, B., Bussjaeger, R.J., Shaheen, G., 2009. Simultaneous, noninvasive observation of elastic scattering, fluorescence and inelastic scattering as a monitor of blood flow and hematocrit in human fingertip capillary beds. J. Biomed. Optic. 14 (5), 050505.

Dingari, N.C., Barman, I., Kang, J.W., Kong, C.-R., Dasari, R.R., Feld, M.S., 2011. Wavelength selection-based nonlinear calibration for transcutaneous blood glucose sensing using Raman spectroscopy. J. Biomed. Optic. 16 (8), 087009.

Kang, J.W., Park, Y.S., Chang, H., Lee, W., Singh, S.P., Choi, W., Galindo, L.H., Dasari, R. R., Nam, S.H., Park, J., So, P.T.C., 2020. Direct observation of glucose fingerprint using in vivo Raman spectroscopy. Sci. Adv. 6 (4), eaay5206.

Kotarski, M., Smulko, J.M., 2009. Assessment of synchronic detection at low frequencies through DSP-based board and PC sound card. Proc. XIX IMEKO World Congress Fundamental and Applied Metrology 960–963.

Lipson, J., Bernhardt, J., Block, U., Freeman, W.R., Hofmeister, R., Hristakeva, M., Lenosky, T., McNamara, R., Petrasek, D., Veltkamp, D., Waydo, S., 2009. Requirements for calibration in noninvasive glucose monitoring by Raman spectroscopy. J. Diabetes Sci. Technol. 3 (2), 233–241.

Lundsgaard-Nielsen, S.M., Pors, A., Banke, S.O., Henriksen, J.E., Hepp, D.K., Weber, A., 2018. Critical-depth Raman spectroscopy enables home-use non-invasive glucose monitoring. PLoS One 13 (5), e0197134.

Ma, K., Yuen, J.M., Shah, N.C., Walsh, J.T., Glucksberg, M.R., Van Duyne, R.P., 2011. In vivo, transcutaneous glucose sensing using surface-enhanced spatially offset Raman spectroscopy: multiple rats, improved hypoglycemic accuracy, low incident power, and continuous monitoring for greater than 17 days. Anal. Chem. 83 (23), 9146–9152.

Pandey, R., Paidi, S.K., Valdez, T.A., Zhang, C., Spegazzini, N., Dasari, R.R., Barman, I., 2017. Noninvasive monitoring of blood glucose with Raman spectroscopy. Acc. Chem. Res. 50 (2), 264–272.

Pezzotti, G., Boffelli, M., Miyamori, D., Uemura, T., Marunaka, Y., Zhu, W., Ikegaya, H., 2015. Raman spectroscopy of human skin: looking for a quantitative algorithm to reliably estimate human age. J. Biomed. Optic. 20 (6), 065008.

Pleus, S., Schauer, S., Jendrike, N., Zschornack, E., Link, M., Hepp, K.D., Haug, C., Freckmann, G., 2021. Proof of concept for a new Raman-based prototype for noninvasive glucose monitoring. J. Diabetes Sci. Technol. 15 (1), 11–18.

Sachdeva, S., 2009. Fitzpatrick skin typing: Applications in dermatology. Indian J. Dermatol. Venereol. Leprol. 75 (1), 93–96.

Scholtes-Timmerman, M.J., Bijlsma, S., Fokkert, M.J., Slingerland, R., van Veen, S.J.F., 2014. Raman spectroscopy as a promising tool for noninvasive point-of-care glucose monitoring. J. Diabetes Sci. Technol. 8 (5), 974–979.

Singh, S.P., Mukherjee, S., Galindo, L.H., So, P.T.C., Dasari, R.R., Khan, U.Z., Kannan, R., Upendran, A., Kang, J.W., 2018. Evaluation of accuracy dependence of Raman spectroscopic models on the ratio of calibration and validation points for non-invasive glucose sensing. Anal. Bioanal. Chem. 410 (25), 6469–6475.

Smulko, J.M., Dingari, N.C., Soares, J.S., Barman, I., 2014. Anatomy of noise in quantitative biological Raman spectroscopy. Bioanalysis 6 (3), 411–421.

Spegazzini, N., Barman, I., Dingari, N.C., Pandey, R., Soares, J.S., Ozaki, Y., Dasari, R.R., 2014. Spectroscopic approach for dynamic bioanalyte tracking with minimal concentration information. Sci. Rep. 4, 7013.

Tuchin, V.V., 2008. Handbook of Optical Sensing of Glucose in Biological Fluids and Tissues. CRC Press.

Wang, C., Li, X., Hu, H., Zhang, L., Huang, Z., Lin, M., Zhang, Z., Yin, Z., Huang, B., Gong, H., Bhaskaran, S., Gu, Y., Makihata, M., Guo, Y., Lei, Y., Chen, Y., Wang, C., Li, Y., Zhang, T., Chen, Z., Pisano, A.P., Zhang, L., Zhou, Q., Xu, S., 2018. Monitoring of the central blood pressure waveform via a conformal ultrasonic device. Nat. Biomed. Eng. 2, 687–695.

Wróbel, M.S., 2016. Non-invasive blood glucose monitoring with Raman spectroscopy: prospects for device miniaturization. IOP Conf. Ser. Mater. Sci. Eng. 104 (1), 012036.

Yamakoshi, K., Yamakoshi, Y., 2006. Pulse glucometry: a new approach for noninvasive blood glucose measurement using instantaneous differential near-infrared spectrophotometry. J. Biomed. Optic. 11 (5), 054028.

Zhou, Z., Padgett, S., Cai, Z., Conta, G., Wu, Y., He, Q., Zhang, S., Sun, C., Liu, J., Fan, E., Meng, K., Lin, Z., Uy, C., Yang, J., Chen, J., 2020. Single-layered ultra-soft washable smart textiles for all-around ballistocardiograph, respiration, and posture monitoring during sleep. Biosens. Bioelectron. 155, 112064.